



**HAL**  
open science

# The robotized laser doppler vibrometer: On the use of an industrial robot arm to perform 3D full-field velocity measurements

Pierre Margerit, Tristan Gobin, Arthur Lebée, Jean-François Caron

## ► To cite this version:

Pierre Margerit, Tristan Gobin, Arthur Lebée, Jean-François Caron. The robotized laser doppler vibrometer: On the use of an industrial robot arm to perform 3D full-field velocity measurements. Optics and Lasers in Engineering, 2021, 137, pp.106363 -. 10.1016/j.optlaseng.2020.106363 . hal-03492244

**HAL Id: hal-03492244**

**<https://hal.science/hal-03492244>**

Submitted on 9 May 2022

**HAL** is a multi-disciplinary open access archive for the deposit and dissemination of scientific research documents, whether they are published or not. The documents may come from teaching and research institutions in France or abroad, or from public or private research centers.

L'archive ouverte pluridisciplinaire **HAL**, est destinée au dépôt et à la diffusion de documents scientifiques de niveau recherche, publiés ou non, émanant des établissements d'enseignement et de recherche français ou étrangers, des laboratoires publics ou privés.

# The Robotized Laser Doppler Vibrometer: on the use of an industrial robot arm to perform 3D full-field velocity measurements

Pierre Margerit<sup>a</sup>, Tristan Gobin<sup>b</sup>, Arthur Lebee<sup>a,\*</sup>, Jean-François Caron<sup>a</sup>

<sup>a</sup>Laboratoire Navier, UMR 8205, École des Ponts, IFSTTAR, CNRS, UPE, Champs-sur-Marne, France

<sup>b</sup>HAL Robotics Ltd.

---

## Abstract

An original experimental setup, dedicated to the measurement of the dynamic response of structures, is presented. Called the Robotized Laser Doppler Vibrometer (RLDV), it consists in the assembly of a fixed point Laser Doppler Vibrometer (LDV) on a 6-axis industrial robot arm. This allows to measure the 3D velocity on the surface of objects with a wide range of shapes and sizes. In comparison with commercially available solutions, it represents an affordable and versatile tool. First, the motivations and the new challenges associated to the use of a robot arm to do such experiments are discussed. Second, the different strategies implemented to overcome these difficulties are developed. A software solution is proposed. By the use of a virtual model of the experimental setup, the measurement procedure can be designed and simulated in order to preview robot motion and avoid collisions. With a small number of parameters, the good proceeding of the measurement can be insured on a fine measurement mesh. The software is completed by an interface that allows for the setting of the signal acquisition parameters. At the end, all the procedure is automated and long measurements can be achieved with a reduced supervision. To illustrate the proposed setup, an experimental application is developed. The 3D modal shapes of a curved beam are measured and compared with numerical predictions, showing an excellent correlation.

**Keywords:** Full-field measurements, Robotics, Laser Doppler Vibrometer

---

## 1. Introduction

During the last few decades, a number of so-called *full-field* measurement techniques were developed: instead of being limited to single-point measurements, physical quantities can now be measured on fine meshes of points, providing insights on their spatial distribution. These techniques usually take advantage of the ability to replicate sensors (e.g cameras) or to move the measurement point location (e.g scanning sensors). Among these new tools, some allow a contactless measurement of the kinematic field of a structure submitted to a dynamic excitation. In the community of structural mechanics, the data redundancy offered by such measurement techniques encouraged the development of identification methods providing rich experimental data for material characterization or model validation [1]. In dynamics, one can mention the Modal Analysis [2], the Force Analysis Technique [3], the Virtual Field Method [4] or the High-Resolution Wavevector Analysis [5, 6].

A popular sensor used to perform dynamical measurements is the Laser Doppler Vibrometers (LDV). It allows the measurement of an object velocity at a fixed point, projected in the direction of the laser beam. In order to perform full-field measurements, the laser beam target position can be controlled with the help of galvo scanners. This is the principle of the Scanning Laser Doppler Vibrometer (SLDV), that is well established as a versatile tool to perform full-field measurement over a wide frequency range [7]. At each location along the mesh of measured points, the experiment is repeated so that the velocity field map can be reconstructed. By comparison to high-speed cameras, no data processing (i.e. optical flow computation) is needed and the proportionality between velocity and displacement magnitudes with frequency improves the signal to noise ratio the high frequency regime. As a counterpart, the use of the SLDV requires a particular attention to the experiment repeatability as the measured point changes. Moreover, when the structural response can be considered steady, Continuous-Scan Laser Doppler Vibrometry (CSLDV) can be implemented in order to speed up acquisition times [8, 9, 10].

---

\*. Corresponding author. [arthur.lebee@enpc.fr](mailto:arthur.lebee@enpc.fr)

Moreover, some identification methods need the measurement of the 3D kinematic field of the structure. As the LDV measures the instantaneous velocity in the direction of its laser beam, one has to perform the velocity measurement for a number of laser incidence angles in order to retrieve the three components of the velocity. As a consequence, either the SLDV head has to be moved [11, 12] or three LDVs have to be used simultaneously [13], thus leading to a high price of the overall setup. Moreover, these solutions requires a number of manual handling steps that limit the number of points that can be measured. In addition, uncertainties can arise from incorrect positioning of the laser head.

Recently, automated solutions were developed in order to overcome these limitations. Using a set of mirrors assembled on a rotary hollow shaft, it has been shown that it is possible to measure the three translations and local rotations (6 DOFs) of a point by implementing continuous scanning along circular paths [14, 15]. Perhaps the most complete solution can be found in [16], where three SLDVs are assembled on the head of an industrial robot arm. However, this commercially available solution is offered at a very high price.

The aim of the present work is to discuss a setup which is able to perform 3D velocity full-field measurements at a reduced price. The idea is to assemble a single point LDV on an industrial robot arm. The weight to be held being reduced, the robot arm can be smaller hence the price kept affordable. The present setup is consequently called the Robotized Laser Doppler Vibrometer (RLDV). A companion software solution is provided with the proposed setup [17]. The first part, integrated in the Rhinoceros CAD software<sup>1</sup> by means of the Grasshopper plug-in, is used to build the *virtual experimental setup*, in which the mesh of measurement points can be defined. The preview and control of the robot motion is implemented by the use of the HAL 5.3 plug-in<sup>2</sup>. The second part of the proposed software solution is devoted to signal acquisition, processing and preview and is implemented in Matlab.

The work is organized as follows: first, a discussion is given about (i) the motivations of performing LDV measurements with an industrial robot arm and (ii) the difficulties that arise when using such device. Second, the proposed software solution is briefly described in order to give an overview of its operation. Third, an experimental application is presented to validate the setup. The 3D mode shapes and frequencies of a curved beam are

measured and compared to predicted mode shapes.

## 2. The Robotized Laser Doppler Vibrometer

A fixed point Laser Doppler Vibrometer measures the instantaneous velocity  $v_k(t)$  in the direction  $\mathbf{n}_k$  of its laser beam (see Figure 1). By moving the LDV, the measurement of the velocity can be performed, at the same point, for  $K \geq 3$  distinct laser incidence vectors  $\mathbf{n}_k$ . As a consequence, the 3D instantaneous velocity  $\mathbf{u}(t) = \tau[u_1(t), u_2(t), u_3(t)]$  of the point, expressed in the cartesian coordinates, can be retrieved:

$$\mathbf{u}(t) = \mathbf{P}^\dagger \mathbf{v}(t) \quad (2.1)$$

where  $\mathbf{P} = [\mathbf{n}_1 \dots \mathbf{n}_K]$  is the transfer matrix,  $\bullet^\dagger$  denotes the matrix pseudo inverse and  $\mathbf{v}(t) = \tau[v_1(t) \dots v_K(t)]$  contains the instantaneous velocity measured for each laser orientation  $\mathbf{n}_k$ . At this point, it can be noted that some LDV sensors include displacement decoder. In this case, retrieving the 3D instantaneous displacement would be straightforward, directly replacing the measured velocities  $\mathbf{v}(t)$  by the obtained displacement in Eq. (2.1).

### 2.1. Motivations

Multiple axis robot arms, originally developed for industrial applications, can manipulate a wide range of tools of different weights and shapes, with speeds, position accuracy and holding loads which make them interesting for a wide number of applications. In particular, a number of reasons motivates the assembly of a LDV on a robot arm.

**Accuracy.** Even with a rough calibration, modern industrial robot arms can position the tool with a sub-millimeter accuracy. Consequently, the uncertainty in the

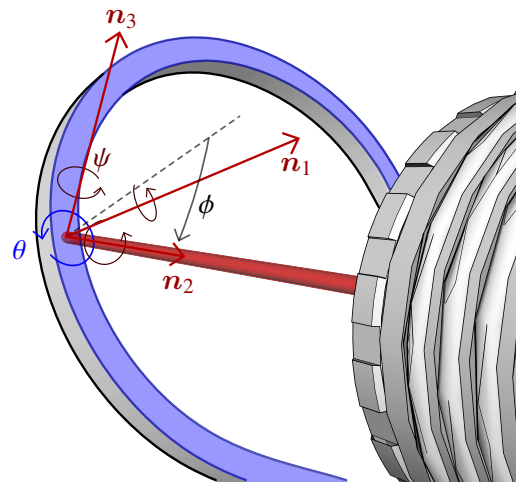


Figure 1: Measurement of the 3D velocity of a point. Laser beam vector basis  $\{\mathbf{n}_i\}$ , orientation of the basis  $\theta$ , incidence angle  $\phi$  and rotation of the LDV around the laser axis  $\psi$ .

1. [www.rhino3d.com/en](http://www.rhino3d.com/en)  
2. [www.hal-robotics.com](http://www.hal-robotics.com)

position  $\mathbf{p}$  of the measured point and the laser beam vectors  $\mathbf{n}_k$  can be reduced, thus lowering the uncertainty in the computed 3D velocity. Indeed, some processing methods based on full-field data make assumptions on the regularity of the measurement mesh [4, 18, 5] that can lead to large bias in the results if not fulfilled.

**Flexibility.** In the procedure of retrieving the 3D components of the velocity (2.1), the choice of the positions of the LDV is critical. Indeed, when  $K > 3$ , the velocity in the cartesian coordinates is estimated in the least-squares sense. Hence the chosen incidence angles  $\phi$  (see figure 1) have an influence on the conditioning of  $\mathbf{P}$ , which is critical in the estimation of  $\mathbf{u}(t)$  (equation (2.1)). In the case  $K = 3$ , the best strategy [19] seems to measure the velocity along directions making an angle of  $45^\circ$  with the object surface's normal at the considered point. Consequently, the laser incidence angles  $\phi$  has to be optimized in order to ensure the good conditioning of the 3D velocity retrieval. In comparison to a Scanning Laser Doppler Vibrometers fixed on a tripod, a fixed Laser Doppler Vibrometer mounted on a 6-axis robot arm offer a lot of flexibility in the positioning of the tool and objects with a wide variety of shapes can be measured.

**Automation.** Being by definition a programmable manipulator, a robot arm can perform automatized measurements. As a consequence, full-field LDV measurements can be achieved on a great number of points with reduced supervision.

## 2.2. New challenges

As a counterpart of the motivations mentioned above, additional complexity arises with the use of a robot arm to perform such measurements. In particular, as the actuated robot arm joints are rotations, the motion of the robot is by far less intuitive than classical cartesian manipulators. Consequently, a number of elements have to be taken into account in the design of an experiment including the use of a robot arm.

**Accessibility.** When using a cartesian manipulator, one can infer the accessibility of one point, as every point on the volume given by the translation axes bounds is theoretically reachable. However, when using a robot arm with only pivot joints, the accessibility of a point cannot be guaranteed, even if it is in the sphere centered in the robot base position and which radius is the total arm length.

**Motion interpolation.** When moving between two robot configurations (the different LDV positions), one has to choose how to interpolate the positions. Based on cartesian manipulator experience, an intuitive way would be to linearly interpolate between two positions in the

cartesian space. However, this type of motion can lead to very large joint rotations near the so-called robot arm *singularities*, thus leading to unwanted motion of the arm. In addition, even if both the start and the end positions are accessible, nothing can guarantee that every linearly interpolated positions in-between can be reached. An alternative choice could be to interpolate linearly between the two joint configurations, in the joint space (rotations). Hence the singularities would be avoided and the accessibility guaranteed. However, this type of motion often leads to large non-intuitive motion in the cartesian space. These so-called *re-orientations* has to be avoided as much as possible, as they can lead to collisions.

**Collisions.** During the robot motion, a number of collisions can occur: (i) the robot with itself; (ii) between the robot and the tool or (iii) with the experiment environment. As the consequences of such collisions can be dramatic for the experiment, any collision has to be avoided.

As a consequence of the added complexity, it is necessary to build a *virtual* model of the experiment, that allows to preview the robot motion, set and optimize the target parameters and perform collision tests. The main problem to be solved when designing a robot setup simulation is the inverse kinematic problem.

**Inverse Kinematics.** A robot setup can be described by a series of frames that define different coordinate systems. In the present application, the laser target is a frame  $\mathcal{F}_p$  (see Fig. 2), given by the laser beam vector  $\mathbf{n}$ , the tar-

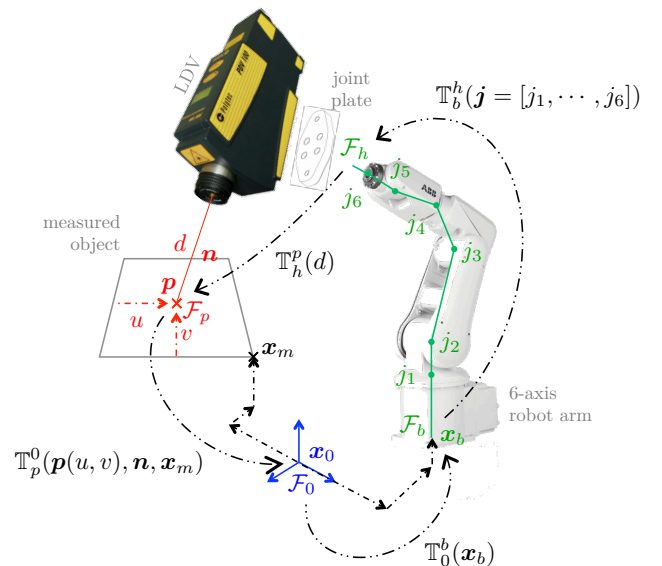


Figure 2: Diagram of the he Robotized Laser Doppler Vibrometer setup with the subsequent

frame transformations  $\mathbb{T}_i^j$  (2.2) defining the kinematic chain (2.3).

geted point  $p$  and an additional angle  $\psi$  which describes the rotation of the frame around  $n$  (see Fig. 1). The target position  $p$  is given by the measured object position  $x_m$  expressed in the (arbitrary) reference frame  $\mathcal{F}_0$  and the normalized coordinates  $(u, v)$  on the surface of the object. The robot is defined by its base frame  $\mathcal{F}_b$ , given by its position  $x_b$  and orientation in the reference frame. Finally, the robot head frame  $\mathcal{F}_h$ , which coincides with the LDV base frame, is given by the 6 robot arm joint rotation angles  $\mathbf{j} = [j_1, \dots, j_6]$ . From two subsequent frames can be defined geometrical transformations:

$$\mathcal{F}_j = \mathbb{T}_i^j \mathcal{F}_i \quad (2.2)$$

The kinematic chain can finally be defined with the identity transformation  $\mathbb{I}$ :

$$\mathbb{I} = \mathbb{T}_0^0 = \mathbb{T}_0^b \mathbb{T}_b^h \mathbb{T}_h^p \mathbb{T}_p^0 \quad (2.3)$$

Let us assume for now that each frame  $\mathcal{F}_i$  is given: the positions of the measured object and robot base are known and the transformation  $\mathbb{T}_h^p$  is computed from the tool geometry and for a given laser beam length  $d$ . While the forward kinematic problem of computing the transformation  $\mathbb{T}_b^h$  from the robot joint values  $\mathbf{j}$  is straightforward, the inverse kinematic problem is more complex:

$$\mathbf{j} = \left\{ \mathbf{a} \in \mathbb{R}^6 \mid a_i \in [j_i^-, j_i^+], \mathbb{T}_b^h(\mathbf{a}) = \left( \mathbb{T}_h^p \mathbb{T}_p^0 \mathbb{T}_0^b \right)^{-1} \right\} \quad (2.4)$$

where the  $j_i^-$  and  $j_i^+$  are respectively the minimum and maximum allowed robot arm joint values. In particular, as the parameters  $\mathbf{j}$  describe rotations, the solution is not unique. In order to simulate the robot motion, an inverse kinematic solver has to be implemented.

### 3. The controlling software

In order to be able to achieve measurements with the RLDV, a software solution has been developed for the present work [17]. It is divided in two parts: the first part is devoted to the modelling of the geometries of the experiment and the control of the robot. The aim of the second part is to handle the setting of the signal acquisition parameters, the signal processing steps, the measurement preview and finally the export of the measurement. A block diagram of the software solution is schematized in Figure 3. Each part is detailed further in the two following subsections.

#### 3.1. The virtual experiment model

The aim of the first part of the implemented software is to help the user of a RLDV setup to design the experiment and ensure the good proceeding of the measurement. It is based on the CAD software Rhinoceros3D<sup>1</sup>, with the Grasshopper plug-in which allows to process geometries via a graphical programming environment. This software configuration allows to model the different geometries of the experiment and process them with routines in order to create the RLDV targets, simulate the robot motion and write the code that is finally sent to the robot controller. The Grasshopper canvas associated to the proposed software [17] implements the different strategies presented in the following paragraphs.

All the steps involving robotic specific tasks are achieved thanks to the HAL plug-in<sup>2</sup>. This tool is dedicated to the design of general robotic setups. It includes an inverse kinematic solver (problem (2.4)), a library of robot arm presets from robot manufacturers, a range of tools dedicated to robot target handling and motion simulation and finally a tool that allows to communicate with the robot controller.

**Geometries of the experiment.** The first step of the design of a RLDV experiment is to create a model of the geometries that will be involved in the measurement. Three types of geometries can be distinguished:

1. Measured objects, used to create the measurement mesh and the laser beam targets.
2. Reference objects, used to calibrate the measurement setup, for example to accurately determine the relative positions  $x_r$  and  $x_m$  of the robot and the measured object (see Figure 2).
3. Environment objects, included in the robot motion simulation in order to avoid collisions.

The refinement of the geometries has to be chosen carefully, as collision tests are computationally intense, with a burden increasing with the complexity of the involved geometries.

**Measurement mesh.** From the measured object geometry can be created the mesh of measurement points  $p$ . Basically, as the LDV measurement is performed on the surface of the object, the positions of the points are given by discrete values of the  $(u, v)$  parameters that describes the surface. A classical way of building the mesh is to choose points that lies on a regular grid of  $(u, v)$  values. However, a number of meshing strategies (e.g. Delaunay mesh) can be chosen since they are implemented in the Grasshopper plug-in.

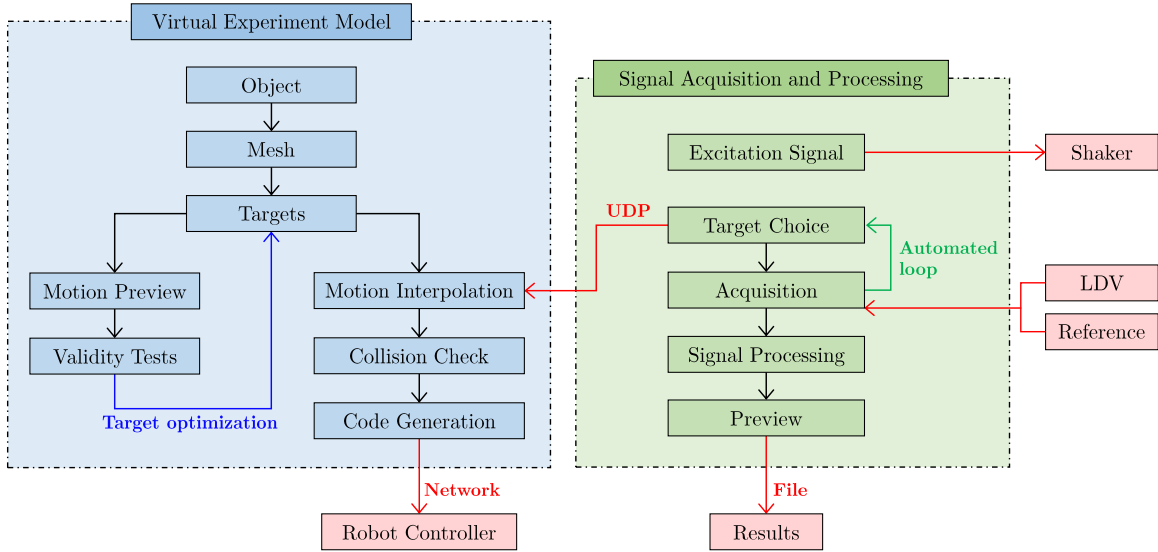


Figure 3: Block Diagram of the proposed RLDV software solution.

**Laser targets.** The next step is concerned by the definition of the laser beam basis  $\mathbf{P} = [\mathbf{n}_1 \dots \mathbf{n}_K]$  (see expression (2.1) and Figure 1). By default, the targets are derived from the measured object surface. First, the normal of the surface of the measured object is evaluated at each measurement point  $\mathbf{p}$ . Second, the  $K$  incident beam vectors are built with the angle shift to normal  $\phi$  as parameter. These vectors are, by default, evenly distributed around the normal. Additionally, the overall target configuration can be rotated of an angle  $\theta$  around the normal (see Figure 1). As not only a vector but a complete frame has to be given to fix the robot configuration, an angle  $\psi$  has to be set in order to define the rotation of the LDV around the laser beam axis. This target definition strategy is indicative and can be shortcut by the user. As a consequence, a wide variety of object can be measured, by adapting the target generation steps.

**Robot motion preview.** Once the targets have been built, the HAL plugin is used to preview the robot motion. At this step, a number of validity tests have to be performed in order to ensure the overall target accessibility. The software computes the inverse kinematics and returns information about the joint configuration of the arm, for each target. Invalid targets (joints out of bounds or unreachable positions) are made visible on the geometrical model. No collision test is performed at this step, as it would involve a high computational burden. The user then has to check for collisions visually.

**Global target parametrization.** In order to make all the targets accessible, the user has to adapt the parameters  $\phi$ ,  $\theta$  and  $\psi$  represented on Figure 1. As a large number

of points are usually measured with such a setup, setting these parameters for each individual target would represent a lot of work. In order to keep the target definition simple, a global parametrization is proposed. Inspired from finite element shape functions, each parameter is set as a function  $f$  of the  $(u(\mathbf{p}), v(\mathbf{p}))$  parameters of the surface at each target point  $\mathbf{p}$ :

$$\begin{aligned}
 f(\mathbf{p}) &= f(u(\mathbf{p}), v(\mathbf{p})) \\
 &= f_1 \times (1 - u(\mathbf{p}))(1 - v(\mathbf{p})) \\
 &+ f_2 \times (1 + u(\mathbf{p}))(1 - v(\mathbf{p})) \\
 &+ f_3 \times (1 - u(\mathbf{p}))(1 + v(\mathbf{p})) \\
 &+ f_4 \times (1 + u(\mathbf{p}))(1 + v(\mathbf{p}))
 \end{aligned} \tag{3.1}$$

with  $(u(\mathbf{p}), v(\mathbf{p})) \in [-1; 1]$ . The user then has only to choose the  $3 \times 4$  parameters  $\{\phi_i, \theta_i, \psi_i\}$  with  $i = 1, \dots, 4$ , while keeping sufficient freedom to make all the targets accessible in an intuitive way. In addition, the laser focus distance  $d$  (distance from the LDV to the object surface, see Figure 1) can be tuned. As the Polytech PDV-100 LDV used in the present work has manual optics,  $d$  is set to be constant. Let us notice that some LDV have remote-controlled optics, that could be used to even increase the freedom given to the user to optimize the target configuration.

Once all set so that they are accessible, the targets can be sent to the second part of the software dedicated to signal acquisition, processing and preview. This second part (presented later) then becomes the master program, and the first part the slave program. When a robot motion is needed, the target to be reached is sent by the master

software to the slave via the *User Data Protocol* (UDP). Before performing the robot motion, additional steps are needed.

**Motion interpolation.** Every motion is basically defined by the starting target and the end target. The right motion interpolation strategy (i.e. in the cartesian or the robot arm joints space) has to be chosen between them in order to ensure the feasibility of the motion task. A mixed approach is proposed. First, additional targets are added between the start and end targets. They are computed by a linear interpolation in the cartesian space. Then, between these targets the robot motion is interpolated in the joint space. As a consequence, both large motions of the arm due to linear interpolation in the joint space between two distant targets and singularities due to linear interpolation in the cartesian space are avoided.

**Collision check.** As the present steps are performed in the automated working mode, collisions have to be checked. Thanks to the chosen motion interpolation strategy, only a few arm positions has to be validated, the computational cost of such test is reduced. If a potential collision is detected for the scheduled motion, this motion is cancelled and the program returns an error.

**Code generation.** Once the trajectory of the robot has been generated and validated, the code necessary to communicate with the robot controller is written by the HAL plugin. Finally, the code is downloaded and the motion task performed directly.

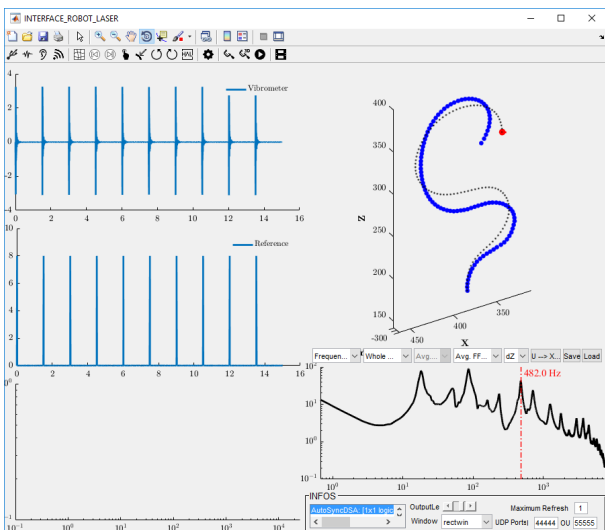


Figure 4: A capture of the Matlab interface, the part of the RLDV software related to signal acquisition, processing and measurement preview.

### 3.2. Signal acquisition and processing

The second part of the software, implemented in Matlab, is devoted to signal acquisition, processing and preview. As it represents classical signal handling routines, only few details are given on these aspects here. A capture of the software interface is given in Figure 4.

A number of excitation signal types are available, both transient (e.g. burst) and stationary (e.g. white noise, blue noise, sweep). The signal processing routines allow to compute various indicators, as the transfer function between the velocity and the reference signals, the coherence, etc.

It has to be noticed that every signal processing step is performed before the 3D velocity determination procedure described in (2.1). Indeed, as this last operation can be badly conditioned, it is preferred to reduce the noise ratio as much as possible before. In addition, this last step induces correlation between the noise associated to each experiment realization, which effects on the measurement uncertainty can be hard to interpret.

Once the targets have been received from the virtual geometrical model, this second part of the software becomes the master program. It then allows to choose a specific target to perform some elementary checks (i.e. signal-to-noise ratio quantification) before starting the measurement. As the overall measurement procedure is automated, long measurements can be performed with a reduced supervision, allowing to achieve measurements on fine meshes of points.

## 4. Experimental validation case

In order to test the validity of the proposed setup, a simple application case study is presented. The modes of a curved beam are measured with the RLDV and the comparison with synthesized modes is performed. As the beam is curved, the mode shapes are expected to contain multiple velocity components. In order to be build with a laser cutting machine, the beam has been chosen so that its neutral axis lays in a plane. As a consequence, this plane is a plane of symmetry of the beam: the modes of the structure are either *contained* in this plane *or* with a dominant out-ofplane component.

The beam of  $b = 5$  mm width is cut on a PMMA plate of  $h = 6$  mm thickness (see Fig. 5). The Young and the shear modulus are respectively  $E = 4.5$  GPa and  $G = 1.5$  GPa.

### 4.1. The model

To validate the measured mode shapes, a curved beam model is implemented. Following the Timoshenko beam

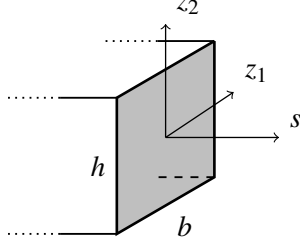


Figure 5: Beam geometry and coordinate axis.  $h = 6$  mm,  $b = 5$  mm.

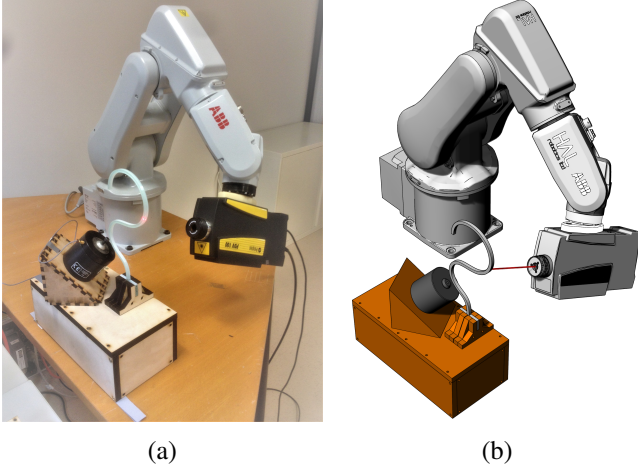


Figure 6: The experimental setup for the validation case study. (a) Picture of the real setup. (b) Screen shot of the virtual setup.

model, the kinematic field is postulated as:

$$\mathbf{u}(s, \mathbf{z}) = \mathbf{w}(s) + \boldsymbol{\alpha}(s) \times \begin{bmatrix} z_1 \\ z_2 \\ 0 \end{bmatrix} \quad (4.1)$$

where  $s$  is the curvilinear coordinate and  $\mathbf{z} = [z_1 \ z_2]$  the position in the beam section (see Fig. 5). By using finite elements, 2064 nodes with 6 degrees of freedom (3 translations  $w_i$ , 3 angles  $\theta_i$ ) are defined. Assuming cantilever boundary conditions (see Figure 6), the first  $N$  numerical modal shapes  $\mathbf{q}$  and frequencies  $\omega$  are obtained so that:

$$\left( \mathbf{K} - \omega_n^2 \mathbf{M} \right) \mathbf{q}_n = 0 \quad , \quad n \in \llbracket 1, N \rrbracket \quad (4.2)$$

#### 4.2. The measurement

**Setup.** The RLDV setup used for this experimental case is composed of a Polytec PDV-100 vibrometer assembled on an ABB IRB 120 industrial robot arm. An assembly plate is inserted between the LDV and the robot head in order to adapt the different screw holes. Both LDV and robot geometries are given by the respective manufacturers and used in the virtual experiment model. The *real* setup and its *virtual* model are represented in Figure 6.

For the signal acquisition, a National Instruments NiDAQ USB-6215 is interfaced with Matlab.

In order to be able to extract the modes of the beam, its free response have to be measured. As the experiment has to be fully automatized, the excitation of the beam has to be sufficiently repeatable. The solution chosen here is to use an electrodynamic shaker as an automatic hammer. At the beginning of each measurement realization, an impulsive electrical signal is sent to the shaker, which consequently hits the beam. This procedure has been found to produce reproducible impact loads with adjustable magnitude and length. In order to excite both in-plane and out-of-plane modes, the shaker is oriented at an oblique angle.

**Target positioning.** The velocity measurement is performed over the top surface of the beam, along the middle curve (see Fig. 5):

$$\mathbf{z} = [0 \ h/2]^\top \quad (4.3)$$

From this curve are extracted  $P = 301$  equally-spaced points that constitute the 1D measurement mesh. Then  $K = 3$  laser targets are defined at each point with a constant incidence angle  $\phi = 25^\circ$ . A 1D version of the shape function 3.1 is used:  $f_{1D}(s) = f(s, 0)$ . Finally, only five parameters ( $\theta_1, \theta_2, \psi_1, \psi_2$  and  $d$  as defined in Fig. 1) need to be set in order to define all the targets.

**Signal acquisition settings.** The maximum observed beam response duration is approximately 0.5 seconds, as the PMMA composing the beam has a high loss factor. Consequently, the experiment duration is set to 0.8 seconds, with a sampling frequency of 51.2 kHz, by far sufficient to avoid aliasing. The excitation signal is sent 10 ms after the beginning of each experiment realization. In order to enhance the signal to noise ratio and to check the experiment repeatability,  $M = 45$  realizations of the experiment are performed for each laser position. Finally, a total of  $M \times K \times P = 45 \times 3 \times 301 = 40635$  experiment realizations are performed, for an overall measurement duration of approximately 20 hours, including the time to move the robot between each target.

**Averaging strategy** When motions perpendicular to the laser beam vector occurs, the LDV sensor is source of speckle noise associated to the measured object's surface roughness. This phenomenon is due to the surface roughness which modifies the instantaneous laser diffraction pattern, thus the quality of the signal received by the LDV. While some Doppler Vibrometer sensors include tracking filters aiming at reducing this source of noise, the proposed solution implements averaging strategies using the ability to repeat the experiment automatically. However, because of the impulsive nature of the speckle noise,

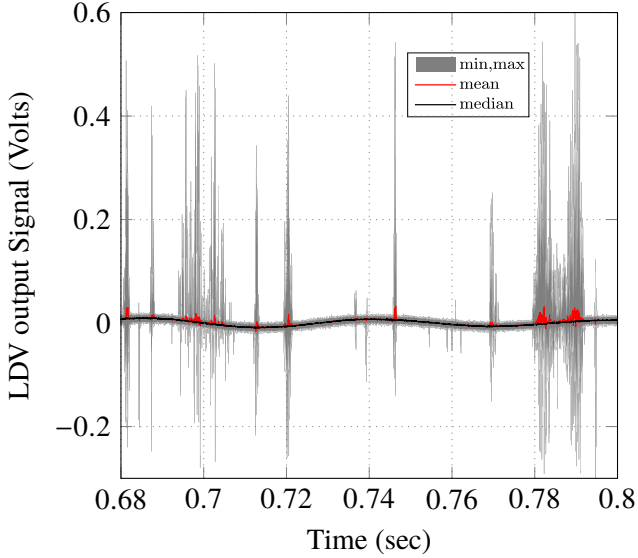


Figure 7: Influence of the averaging steps on 45 realizations of the same measurement: range of the acquired velocities at each time sample (gray patch), mean over the realizations (red line) and median of the realizations (black line).

taking the mean over the  $M$  experiment realizations is not always relevant. Instead, it has been chosen here to compute, at each time sample, the median over the  $M$  available measurements. Hence realizations that contains high impulsive noise are discarded. Figure 7 illustrates the different strategies. It can be observed that the minimum and maximum measured values at each samples (gray envelope) have a very high magnitude compared to the signal amplitude. In addition, even with 45 realizations, the mean value (red line) remains sensitive to these variations. However, the median value (black line) reduces significantly the impulsive noise.

This noise reduction strategy is performed before the 3D velocity estimation procedure (2.1), as impulsive noise would introduce a large bias on this estimation.

As a result of the measurement, the mean absolute velocity over the points is represented in Figure 8. The three cartesian components of the velocity are plotted. From this results can be distinguished the two mode types: out-of plane modes have a dominant  $u_y$  component (orange spectrum), while in-plane modes are composed of both  $u_x$  and  $u_z$  components (resp. blue and yellow spectra).

#### 4.3. Modal analysis

In order to identify the natural frequencies and mode shapes of the beam, an High-Resolution Modal Analysis [2, 20, 21] is performed on the measured velocity 3D field. The modal analysis procedure is applied on the complete set of acquired data, in order to extract the modal

frequencies, the modal dampings and the modal shapes simultaneously. The selection of the number of modes to keep is achieved using a stabilization diagram [22]. Only the 12 first modes of the beam are kept for the comparison, ranging from 10 Hz to 1 kHz. Identified modal frequencies, denoted as vertical gray lines, are labelled in the figure 8. It can be seen that the two first modes are close in frequency ( $f_a = 15.5$  Hz and  $f_b = 17.5$  Hz). The separation of these two modes is made easier by their different displacement components: the first is an out-of-plane mode while the second is dominated by in-plane components of the motion. The corresponding mode shapes are represented in Figure 10.

#### 4.4. Result comparison

To make the comparison between mode shapes obtained from the RLDV measurement and the predicted mode shapes, one has to define the *observation matrix*  $\mathbf{C}$  that projects the nodal displacements  $\mathbf{q}_n$  computed with the model (4.2) on the measurement mesh, so that:

$$\mathbf{u}_n = \mathbf{C}\mathbf{q}_n \quad (4.4)$$

where  $\mathbf{u}_n$  is the  $n^{\text{th}}$  numerical modal vector evaluated on the measurement points. This observation matrix takes into account the contribution of the computed local beam rotation  $\alpha$  in the velocity  $\mathbf{u}$  of the measurement point on the top surface of the beam; from (4.1) and (4.3):

$$\mathbf{u}(s) = \dot{\mathbf{w}}(s) + \frac{h}{2} \begin{bmatrix} \dot{\alpha}_2(s) \\ -\dot{\alpha}_1(s) \\ 0 \end{bmatrix} \quad (4.5)$$

Defining a measured modal shape  $\tilde{\mathbf{u}}_i$  and the numerical mode  $\mathbf{u}_j$ , one can express the *Modal Assurance Criterion* matrix (MAC) as the normalized correlation coefficient between the two shapes:

$$\text{MAC}_{ij} = \frac{\tilde{\mathbf{u}}_i \cdot \mathbf{u}_j}{\|\tilde{\mathbf{u}}_i\| \|\mathbf{u}_j\|} \quad (4.6)$$

The magnitude of the MAC matrix, computed from the 12 experimental modes ("a" to "l") extracted from the measurement and the 16 first modes computed with the beam model (1 to 16), is shown in Figure 9. The measured and the predicted modal shapes are very close, with a mean correlation coefficient of 99%. In Figure 10, the measured (round markers) and the predicted shapes (red lines) are superimposed, for each individual mode. The reference configuration is shown as a black dashed line. It can be seen that the shapes match closely, for both in-plane and out-of-plane modes.

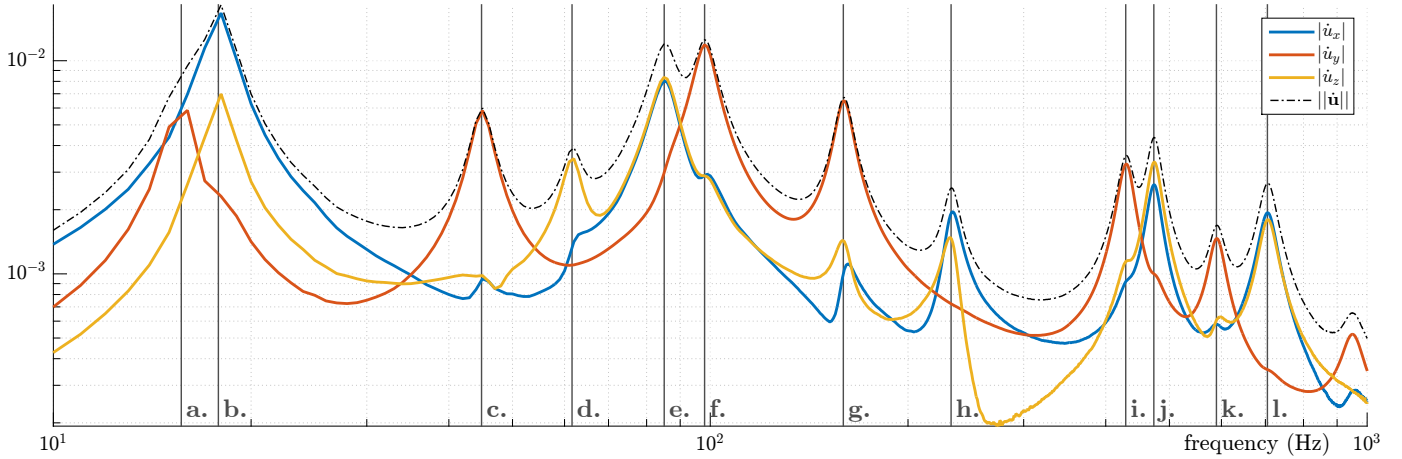


Figure 8: Measurement Results. Root Mean Squared Velocity: magnitude (dashed black line). and cartesian components (colored lines). Identified modal frequencies: vertical gray lines

## 5. Conclusion and Perspectives

An original experimental setup called the Robotized Laser Doppler Vibrometer (RLDV) has been presented. By assembling a single point Laser Doppler Vibrometer (LDV) on an industrial 6-axis robot arm, one is able to perform 3D velocity measurements in an automated way. In comparison to commercially available solutions, the setup is more affordable. By the use of a robot, the accuracy and flexibility of the LDV positioning is improved. Thus, objects with a wide variety of shapes and sizes can be measured. However, the use of a 6-axis robot introduces complexity, which was discussed in the second section of the work. To tackle potential issues associated to robot motion, collisions with surrounding objects or automated code generation, a virtual model of the experiment

is built in order to simulate the robot motion and ensure the good proceeding of the experiment. An implementation of the proposed procedures is available freely [17], using Matlab scripting for signal acquisition and processing and Rhino/Grasshopper/HAL for geometry definition and robotic-specific tasks. In order to illustrate an application of the setup, an experimental case was presented. The 3D mode shapes of a curved beam have been measured and compared to numerical predictions. It has been shown that measured and computed shapes are very close, with a correlation coefficient close to 1.

The experimental setup presented in this work has proven to be a versatile tool allowing the measurement of the dynamic response of a variety of objects [21], for a relatively affordable price. As for now, no investigation has been led on the uncertainties related to the use of a robot. As a perspective, two main uncertainty sources can be given:

**Calibration.** The robotized manipulator insures a *relative* positioning accuracy. However, a good *absolute* positioning accuracy can be hard to obtain, as the position of the robot and the measured object are given with some uncertainty. Until now, a visual check of the laser target position on several points over the measured object has proven to be sufficient to adjust and validate the positions of the different objects in the virtual setup. Nonetheless, a more accurate calibration procedure may be necessary for more demanding object geometries or experimental environments.

**Vibration of the arm.** The 6-axis robot arm cannot be considered infinitely stiff. A procedure could be designed in order to evaluate the contribution of the robot arm vibration in the measured velocity. In the present

|                    |   | Numerical Modes |      |      |      |      |      |      |      |      |      |      |      |      |      |      |     |
|--------------------|---|-----------------|------|------|------|------|------|------|------|------|------|------|------|------|------|------|-----|
|                    |   | 1               | 2    | 3    | 4    | 5    | 6    | 7    | 8    | 9    | 10   | 11   | 12   | 13   | 14   | 15   | 16  |
| Experimental Modes | a | 99.4            | 3.0  | 6.5  | 2.0  | 1.0  | 2.1  | 1.2  | 2.7  | 2.0  | 1.0  | 1.5  | 1.2  | 4.5  | 1.3  | 2.3  | 0.1 |
|                    | b | 4.6             | 99.7 | 9.4  | 1.6  | 1.4  | 1.5  | 1.7  | 1.2  | 4.1  | 4.4  | 0.3  | 4.1  | 3.2  | 1.1  | 3.6  | 0.4 |
|                    | c | 5.8             | 6.5  | 98.8 | 5.1  | 7.2  | 5.3  | 4.7  | 1.1  | 2.2  | 0.4  | 2.7  | 1.5  | 2.3  | 1.5  | 1.2  | 1.2 |
|                    | d | 2.2             | 0.8  | 1.8  | 99.5 | 5.7  | 6.1  | 16.1 | 3.4  | 12.4 | 4.3  | 6.5  | 2.4  | 11.2 | 1.6  | 13.1 | 1.7 |
|                    | e | 2.2             | 5.3  | 3.2  | 1.7  | 99.6 | 1.0  | 2.9  | 0.7  | 1.6  | 0.6  | 8.2  | 2.2  | 7.1  | 3.6  | 5.4  | 1.9 |
|                    | f | 4.9             | 0.3  | 2.2  | 6.6  | 8.4  | 99.4 | 7.0  | 1.6  | 10.1 | 2.3  | 1.2  | 1.4  | 4.2  | 3.3  | 1.2  | 2.6 |
|                    | g | 3.5             | 5.5  | 1.7  | 17.8 | 6.0  | 1.4  | 99.1 | 4.2  | 4.3  | 3.3  | 5.9  | 0.4  | 2.9  | 3.2  | 2.6  | 1.1 |
|                    | h | 1.3             | 1.2  | 0.5  | 3.1  | 1.6  | 0.9  | 8.9  | 99.8 | 7.1  | 2.6  | 17.0 | 2.5  | 10.1 | 4.1  | 7.0  | 8.3 |
|                    | i | 1.4             | 3.8  | 7.5  | 15.2 | 1.4  | 6.1  | 6.8  | 8.4  | 98.6 | 3.8  | 12.0 | 13.5 | 10.1 | 0.8  | 4.0  | 1.8 |
|                    | j | 0.2             | 5.2  | 0.9  | 4.1  | 2.1  | 3.4  | 1.2  | 5.3  | 4.3  | 99.4 | 13.4 | 5.9  | 9.1  | 1.8  | 18.3 | 0.8 |
|                    | k | 3.5             | 0.5  | 6.5  | 11.1 | 5.0  | 4.9  | 2.4  | 23.2 | 8.2  | 13.6 | 97.1 | 2.2  | 12.0 | 2.1  | 10.5 | 9.8 |
|                    | l | 0.4             | 5.4  | 1.9  | 2.5  | 3.1  | 1.4  | 0.2  | 5.7  | 13.0 | 7.0  | 1.7  | 98.2 | 3.9  | 13.5 | 2.2  | 2.4 |

Figure 9: Magnitude of the Modal Assurance Criterion matrix (%) between experimental and numerical modes.

work, this contribution has been neglected. In addition, some robot arms have brakes that can be activated during the signal acquisition step, thus reducing the vibration due to the actuators at the joints.

In the present work, the focus was on LDV measurements. However, the assembly of any sensor on a robot arm could potentially benefit to a wide variety of measurements [23].

## Acknowledgments

This work is part of the ANR founded (french National Research Agency) project MAESTRO (*Modélisation Et Synthèse Sonore pour Tables d'harmonie de piano*, ANR-14-CE07-0014).

## References

- [1] S. Avril, M. Bonnet, A. S. Bretelle, M. Grédiac, F. Hild, P. Ienny, F. Latourte, D. Lemosse, S. Pagano, E. Pagnacco, F. Pierron, Overview of identification methods of mechanical parameters based on full-field measurements, *Experimental Mechanics* 48 (4) (2008) 381–402.
- [2] K. Ege, X. Boutillon, B. David, High-resolution modal analysis, *Journal of Sound and Vibration* 325 (4-5) (2009) 852–869.
- [3] Q. Leclère, F. Ablitzer, C. Pézerat, Practical implementation of the corrected force analysis technique to identify the structural parameter and load distributions, *Journal of Sound and Vibration* 351 (2015) 106–118.
- [4] F. Pierron, M. Grediac, *The Virtual Fields Method*, Springer, 2011.
- [5] P. Margerit, A. Lebé, J.-F. Caron, X. Boutillon, High Resolution Wavenumber Analysis (HRWA) for the Mechanical Characterisation of Viscoelastic Beams, *Journal of Sound and Vibration* 433.
- [6] P. Margerit, A. Lebé, J.-F. Caron, K. Ege, X. Boutillon, High-Resolution Wavevector Analysis for the characterization of the dynamic response of composite plates, *Journal of Sound and Vibration* 458.
- [7] S. J. Rothberg, M. S. Allen, P. Castellini, D. D. Maio, J. J. J. Dirckx, D. J. Ewins, B. J. Halkon, P. Muyschondt, N. Paone, T. Ryan, H. Steger, E. P. Tomasini, S. Vanlanduit, J. F. Vignola, An international review of laser Doppler vibrometry : Making light work of vibration measurement, *Optics and Lasers in Engineering* 99 (October 2016) (2017) 11–22.
- [8] A. B. Stanbridge, D. J. Ewins, Measurement of total vibration at a point using a conical-scanning ldv., in: *Second International Conference on Vibration Measurements by Laser Techniques: Advances and Applications*, Vol. 2868, 1996, pp. 126–136.
- [9] B. J. Halkon, S. Rothberg, Vibration measurements using continuous scanning laser doppler vibrometry: theoretical velocity sensitivity analysis with applications, *Measurement science and technology* 14 (3) (2003) 382.
- [10] M. Martarelli, D. J. Ewins, Continuous scanning laser doppler vibrometry and speckle noise occurrence, *Mechanical Systems and Signal Processing* 20 (8) (2006) 2277–2289.
- [11] P. O. Malley, T. Woods, J. Judge, J. Vignola, Five-axis scanning laser vibrometry for three-dimensional measurements of non-planar surfaces, *Measurement Science and Technology* (20).
- [12] D. Kim, H. Song, H. Khalil, J. Lee, S. Wang, K. Park, 3-D vibration measurement using a single laser scanning vibrometer by moving to three different locations, *IEEE Transactions on Instrumentation and Measurement* 63 (8) (2014) 2028–2033.
- [13] T. Miyashita, Y. Fujino, Development of 3D vibration measurement system using laser doppler vibrometers, in: *Proceedings of SPIE - The International Society for Optical Engineering*, 2006.
- [14] P. Giuliani, D. D. Maio, C. W. Schwingshackl, M. Martarelli, D. J. Ewins., Six degrees of freedom measurement with continuous scanning laser doppler vibrometer., *Mechanical Systems and Signal Processing* 38 (2013) 367–383.
- [15] P. Giuliani, D. D. Maio, C. W. Schwingshackl, M. Martarelli, D. J. Ewins., Experimental validation of a newly designed 6 degrees of freedom scanning laser head: Application to three-dimensional beam structure., *Review of Scientific Instruments* 12 (2013) 121708.
- [16] D. E. Oliver, M. Schuessler, P. Gmbh, Automated Robot-Based 3D Vibration Measurement System, *Sound and Vibration* (April) (2009) 12–15.
- [17] P. Margerit, [Code for the Robotized Laser Doppler Vibrometer](https://doi.org/10.5281/zenodo.3947795) (2020). doi:10.5281/zenodo.3947795. URL <https://doi.org/10.5281/zenodo.3947795>
- [18] F. Ablitzer, C. Pézerat, J.-M. Génevaux, J. Bégué, Identification of stiffness and damping properties of plates by using the local equation of motion, *Journal of Sound and Vibration* 333 (9) (2014) 2454–2468.
- [19] H. Khalil, D. Kim, J. Nam, K. Park, Accuracy and noise analyses of 3D vibration measurements using laser Doppler vibrometer, *Measurement* 94 (2016) 883–892.
- [20] M. Rébillat, X. Boutillon, Measurement of relevant elastic and damping material properties in sandwich thick plates, *Journal of Sound and Vibration* 330 (25) (2011) 6098–6121.
- [21] P. Margerit, Caractérisation large bande du comportement dynamique linéaire des structures hétérogènes viscoélastiques anisotropes. Application à la table d'harmonie du piano., Ph.D. thesis, Université Paris-Est (2018).
- [22] E. Reynders, J. Houbrechts, G. D. Roeck, Fully automated (operational) modal analysis, *Mechanical Systems and Signal Processing* 29 (2012) 228–250.
- [23] M. Nolan, S. A. Verburg, J. Brunskog, E. Fernandez-Grande, Experimental characterization of the sound field in a reverberation room, *The Journal of the Acoustical Society of America* 145 (4) (2019) 2237–2246.

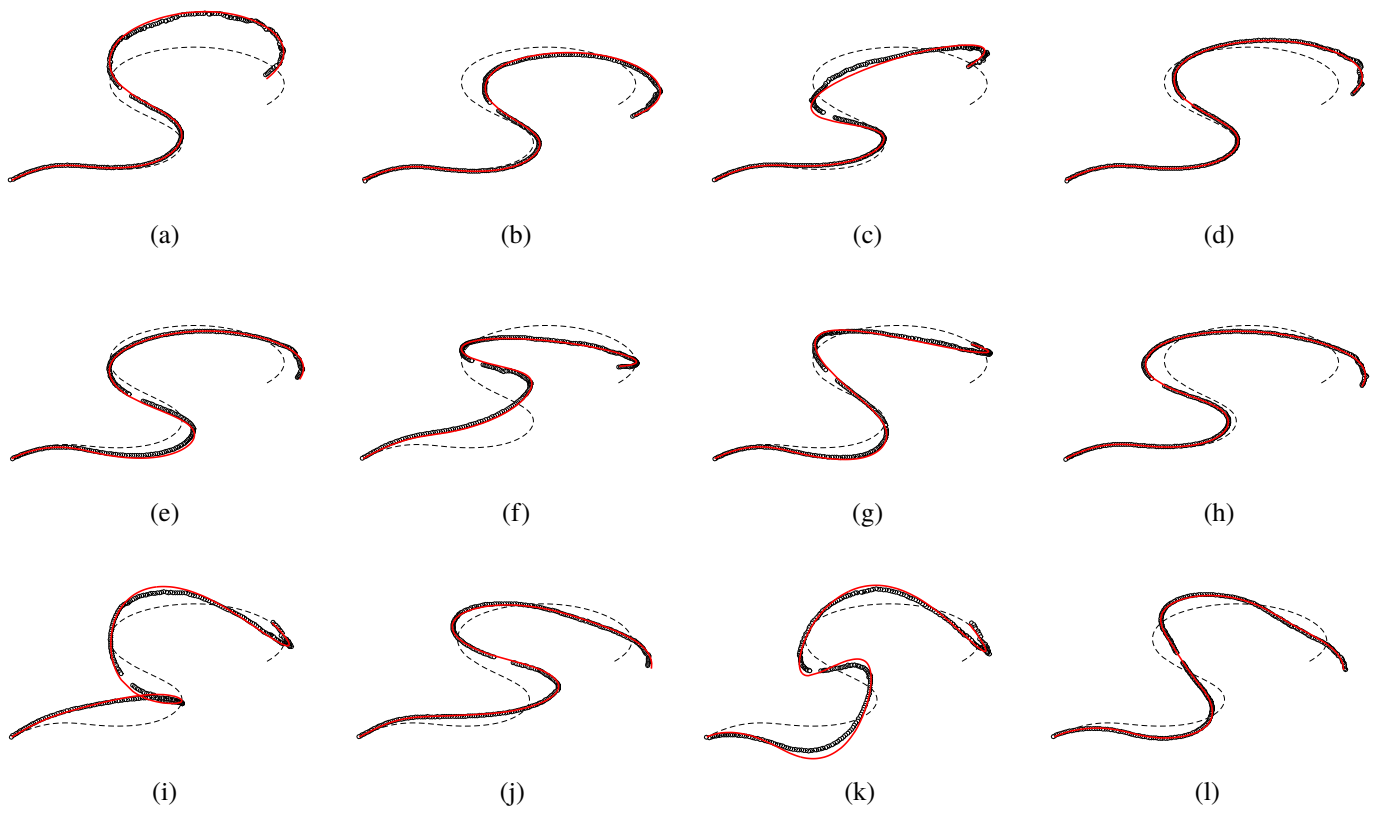


Figure 10: Comparison of experimental (black dots) and numerical mode shapes (red line).